Letter

Emergence of near room-temperature superconductivity in hydrides with H_2 molecular units

Zhao Liu,[1] Junda Li,[1] Eva Zurek,[2] Quan Zhuang,[3] Yanhui Liu,[1,*] Jincheng Yue,[1] Siqi Guo,[1] Ao Zhang,[1] Zhenhua Chi,[1] Xiaoli Huang,[4] and Tian Cui[1,4,†]

[1]*Institute of High Pressure Physics, School of Physical Science and Technology, Ningbo University, Ningbo 315211, People's Republic of China*

[2]*Department of Chemistry, State University of New York at Buffalo, Buffalo, New York 14260-3000, USA*

[3]*Inner Mongolia Key Laboratory of Carbon Nanomaterials, Nano Innovation Institute (NII), College of Chemistry and Materials Science, Inner Mongolia Minzu University, Tongliao 028000, People's Republic of China*

[4]*State Key Laboratory of Superhard Materials, College of Physics, Jilin University, Changchun 130012, People's Republic of China*

(Received 25 May 2023; revised 1 February 2024; accepted 16 February 2024; published 3 May 2024)

The achievement of high-temperature superconductivity in compressed hydrides with extended lattices, e.g., H_3S and LaH_{10}, has become a milestone in the quest for room-temperature superconductivity. For realizing room-temperature superconductivity, lattices where hydrogen adopts multicentered bonds are deemed as indispensable, while hydrides containing H_2 molecular units are believed to be unfavorable. Here, we report H_2 molecular type hydrides with an exceptional near room-temperature superconductivity of 270 K in compressed NaH_{10} and a T_c of 152 K in NaH_{12}, where H atoms solely constitute H_2 units, and Na-H forms ionic bonds. Our first-principles calculations unveil that the high T_c is mainly attributed to strong electron-phonon coupling stemming from the large electron-phonon matrix element driven by medium-frequency interatomic interactions and high-frequency H-derived phonon softening caused by Fermi surface nesting, thus scattering itinerant electrons to form Cooper pairs. Of particular note, we reveal that the unique delocalized background charges cooperate with other electrons occupying the pressure-induced *sp*-hybridized antibonding bands of molecular H_2 units, acting as itinerant electrons to mediate metallic interactions and participate in electron-phonon coupling. This observation reshapes the understanding of superconductivity dominated by molecular H_2 units, provides insights for elucidating phonon-mediated superconductivity, and raises broad prospects of realizing room-temperature superconductivity in molecular hydrogen-based superconductors.

DOI: 10.1103/PhysRevB.109.L180501

The quest for new superconducting materials and the elucidation of their microscopic mechanism of superconductivity has been a grand challenge [1,2] ever since the first ground breaking experiments of Onnes. Ashcroft proposed that the lightest element, hydrogen, would evolve into a metallic solid phase at high pressures, and its high phonon frequencies and robust electron-phonon coupling (EPC) would be a key ingredient required to achieve high-T_c phonon-mediated superconductivity [3]. Despite great experimental strides, it is still debated if a high-pressure phase of solid metallic hydrogen has been made in diamond anvil cells, and the huge pressures required to metallize hydrogen in the solid have challenged the capability of current experiments [4,5]. Hydrides, subsequently, were selected as alternative candidate materials for exploring high-T_c superconductivity ever since Ashcroft proposed that chemical precompression [3,6] can lower the pressure required for metallization. Extensive theoretical studies have predicted a number of binary hydrides with high critical superconducting temperatures (T_c's), finding two general classes of superconducting materials [7–12]. The first includes *p*-block elements that bond with hydrogen covalently in novel proportions, for example, H_3S, which was the first hydride found experimentally and theoretically nearly simultaneously to attain a record-breaking T_c of 203 K at 155 GPa [7,13]. The second includes electropositive metal elements whose valence electrons are transferred to hydrogenic lattices. In particular, experiments have verified predictions of high-T_c superconductivity in phases with clathratelike lattices such as YH_9 (243 K at 200 GPa), LaH_{10} (260 K at 180 GPa) [14–19], and CaH_6 (215 K at 172 GPa) [20,21]. These three-dimensional clathratelike hydrogen lattices, with multicentered hydrogen bonds, are deemed as being indispensable to exceptional superconductivity [2].

However, with the exception of molecular hydrogen, hydrides that contain H_2 units are not known to possess the highest T_c under pressure. The predicted T_c of molecular H-III phase (*Cmca*-12) is 242 K at 450 GPa [22]. The H_2 unit constituted *Ama*2-GeH_4 and $P6_3/mmc$-SnH_4 phases are predicted to possess T_c's of 57 and 62 K, and H_2 units are considered to play a dominant role in improving the EPC [23,24]. In addition, $SiH_4(H_2)_2$ and $GeH_4(H_2)_2$ containing more H_2 molecule units are synthesized with theoretically predicted T_c's of 107 and 90 K [25,26]. Nevertheless, the near room-temperature superconductivity is never obtained in H_2 molecular hydrides and, instead, hydrides containing H_2 units have recently been regarded as an unfavorable factor

*liuyanhui@nbu.edu.cn
†cuitian@nbu.edu.cn

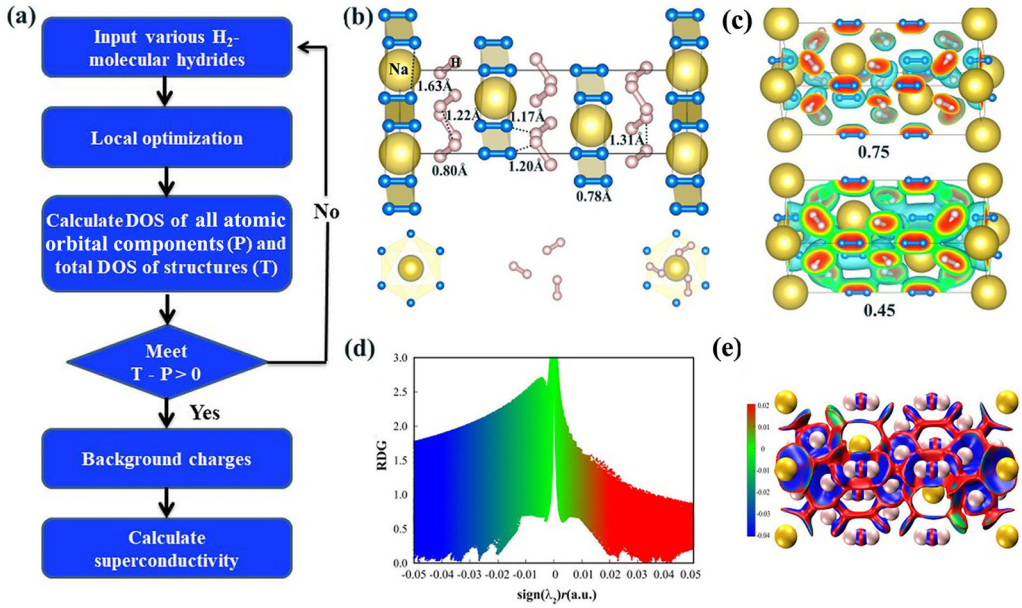

FIG. 1. (a) Schematic illustrating the methodology for identifying potential H_2 molecular type hydrides with high T_c. (b) The $R32$-NaH_{10} phase at 300 GPa and (c) three-dimensional isosurface of the electron localization function (ELF). (d), (e) Plots of the reduced density gradient (RDG) vs electron density (ρ) in terms of the sign of the second Hessian eigenvalue (λ_2) [47].

for superconductivity [2,27]. Whether the H_2 molecular structure can induce a robust EPC and (near) room-temperature superconductivity in hydrides has not yet been determined and remains challenging.

The metallization of phases containing H_2 units can be understood via considering the knowledge of compressed alkali metal polyhydrides [28]. Being attributed to the transfer of valence electrons from the electropositive metal to H_2-σ^* orbitals thus partially filling the H_2-σ^* bands, the R-3m-LiH_6 phase generated a high density of states (DOS) at the Fermi level (ε_F). Meanwhile, "Madelung precompression" generated a smaller volume than what would be expected at relatively low pressures [28]. The pressure-induced broadening and overlap of H^- and H_2-σ^* bands metallize the Pm-NaH_9 phase [29,30]. In KH_5 and RbH_5 species with H_3^- counteranions and H_2 bystander molecules, metallization occurred via pressure-induced widening and the final overlapping of the filled H_3^- nonbonded band with the metal d bands [6,31,32]. The potential T_c of phonon-mediated H_2 molecular type hydrides is markedly influenced by the DOS at ε_F. Intriguingly, we noticed an additive inconsistency between the total DOS and the sum of discrete DOS for different elements in the electronic structure of SbH_4 [33], which are composed of H_2 units (see Fig. S1 in the Supplemental Material [34]). This discrepancy results in the emergence of novel background charges [33,46]. To investigate whether the background charge as a free electron participates in the EPC and induces high-temperature superconductivity holds significant research value in elucidating phonon-mediated superconductivity for H_2 molecular type hydrides. Herein, we proposed a high-throughput structural search approach to screen H_2 molecular type hydrides to quickly identify potential high-T_c superconductors based on the presence of background charges near the ε_F [see Fig. 1(a)]. Application of the proposed method identified and confirmed H_2 molecular type hydrides NaH_{10}, TeH_4, and SnH_{14} possessing background charges near the ε_F [30,33,48]. We take the compressed NaH_{10} as representatives to investigate superconductivity, elucidate the influence of background charges on superconducting behavior, and tackle the challenge of achieving room-temperature superconductivity in H_2 molecular type hydrides.

In this Letter, we confirm a pressure-induced H_2 molecular type superconductor, NaH_{10}, with a T_c of 270 K at 4 Mbar, possessing an unexpected near room-temperature superconductivity. Our first-principles calculations illustrate that large electron-phonon matrix elements are driven by the diverse medium-frequency interatomic interactions, aided via high-frequency H-derived phonon softening caused by FS nesting that scatters itinerant electrons to form Cooper pairs. Notably, these itinerant electrons partially act as delocalized background charges and partially occupy the pressure-induced sp-hybridized antibonding bands of H_2 units to participate in EPC. Further testing the presence of H_2 molecular type hydrides on the resulting superconductivity, we doped sodium into the H-III phase. Our computational experiment yielded a dynamically stable R-3m-NaH_{12} structure with a T_c of 154 K at 150 GPa, where itinerant electrons occupied sp-hybridized orbitals showing delocalized characteristics. These results demonstrate that near room-temperature superconductivity is indeed possible in H_2 molecular type hydrides. Our study reshapes the traditional understanding of superconductivity dominated by H_2 units and provides insights for elucidating phonon-mediated superconductivity in molecular hydrogen based superconductors.

Our enthalpy calculation identified that molecular hydride NaH_{10} is stabilized above 200 GPa with dynamical stability and has a relatively higher enthalpy than $NaH_9 + 1/2H_2$ compounds [49] (see Fig. S2 and Scheme S2 in the Supplemental Material [34]). Notably, NaH_{10} lives on the convex hull when the pressure is above 360 GPa. At 300 GPa, the

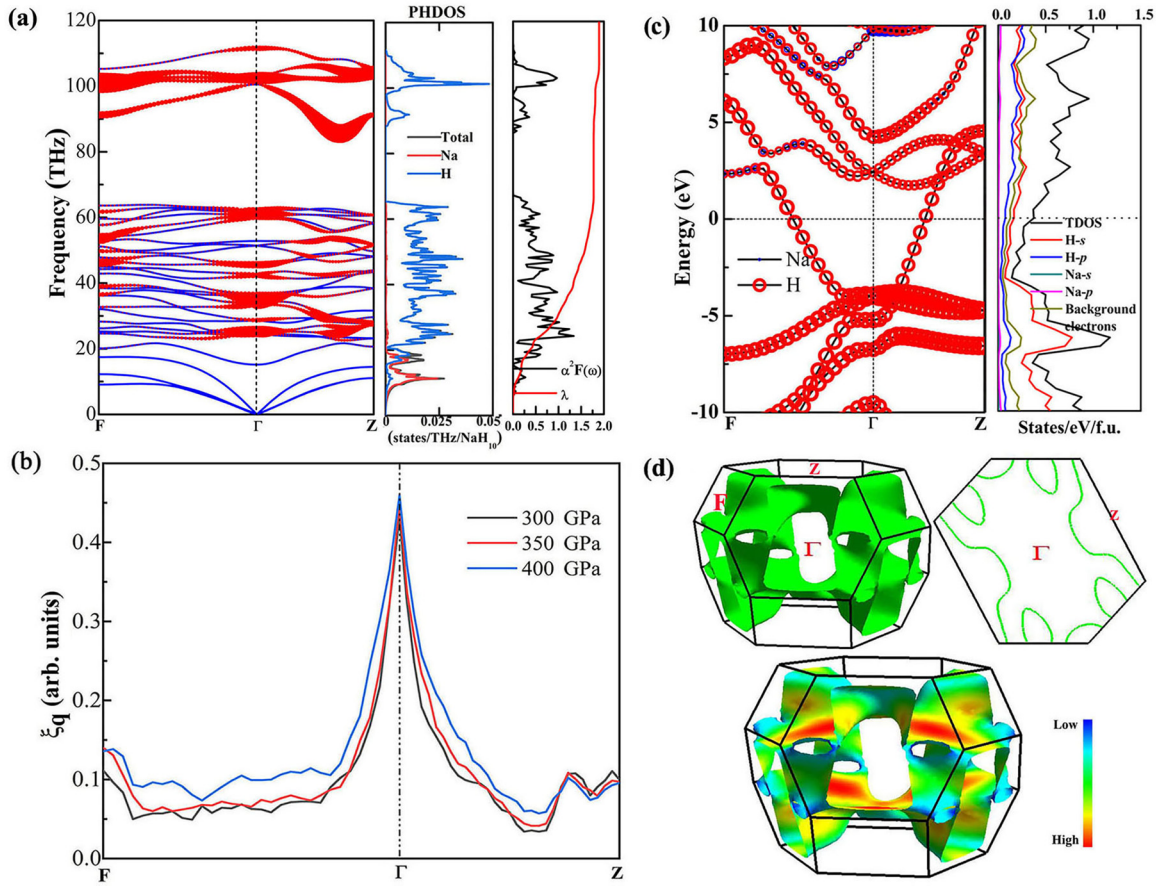

FIG. 2. (a) Phonon dispersion curves, phonon density of states (DOS), and Eliashberg spectral function $\alpha^2F(\omega)$ together with the integral $\lambda(\omega)$ of the $R32$-NaH_{10} phase at 300 GPa. The size of the solid dot on phonon spectra signifies the contribution to the linewidth. (b) The calculated nesting function $\xi_{\boldsymbol{q}}$ with pressure evolution along special $\boldsymbol{q}$ trajectories. (c) Electronic band structure and projected DOS. (d) The FS (upper) and corresponding Fermi velocity (bottom).

H−H bond lengths of 0.78–0.80 Å indicate typical H_2 molecular characteristics, as shown in Fig. 1(b) [23]. Along the c axis, this structure includes three alternate layers of sodium intercalated hydrogen molecules, three-molecule rings with unbound molecular hydrogen and elongated H_2 molecules. The distance between adjacent H_2 units, >1.17 Å, is much larger than the bond length of H_2 gas at ambient conditions, 0.75 Å. The Na−H distance falls between 1.67 and 2.72 Å, suggesting that NaH_{10} is an ionic crystal. In Fig. 1(c), there is no electron localization function (ELF) value at the interval of the H_2 units when the isosurface of 0.75 is adopted, suggesting that there are no covalent interactions. However, metallic bonds have been formed in Fig. S3 [34], as evidenced by the distribution of the free electrons at an isovalue of 0.45.

To reveal the precise interactions between H_2 units, we calculated the key index, the reduced density gradient (RDG), defined as $1/6\pi^2|\nabla\rho|/\rho^{4/3}$ in Fig. 1(d), where ρ represents the electron density. Abundant spikes have large negative values of sign$(\lambda_2)\rho$, and RDG trends to zero, characterizing the noncovalent interactions between H_2 units [50]. For the symmetrical distribution of weak chemical bonding, the vdW interactions located in a ρ range of −0.01–0.01 a.u. with negative and positive values of sign(λ_2). The apparent spikes of RDG corresponding to sign$(\lambda_2)\rho$ associated with positive sign(λ_2) value greater than 0.03 a.u. indicate that steric effects, i.e., repulsive interactions, exist in intermolecular positions of H_2 units, implying that there are electrons occupying its antibonding molecular orbital. These results are also confirmed in Fig. 1(e), where the colors of dark blue and red correspond to attractively ionic and repulsively electrostatic interactions, respectively.

To estimate the superconductivity of the $R32$ phase, we have applied the Allen-Dynes modified McMillan equation based on harmonic approximation to calculate the T_c [51]. For pressure at 300 GPa, the phonon dispersion curves, partial phonon DOS, $\alpha^2F(\omega)$, and EPC λ are displayed in Fig. 2(a). The high-frequency phonons corresponding to the vibration modes of H_2 units are confirmed in Fig. S4 [34], reflecting that this phase is mainly composed of H_2 units. The high-frequency vibrations are consistent with the vibrational frequencies of molecular hydrogen in the H-III phase, especially above 90 THz, which is vastly different from the $I4_1/amd$-H-IV phase of metallic hydrogen containing atomic-H sublattices at 500 GPa [52,53]. Combined with the $\alpha^2F(\omega)$ and the partial phonon DOS analysis, the most significant contributions, ∼80% to the EPC, stem from diverse interatomic interactions identified in Fig. S4 [34], accumulated in medium-frequency vibration modes within 25–65 THz. On the other hand, the vibration modes above 90 THz only

contribute 6.36% to EPC. Medium-frequency optical phonon vibrations play a major role in scattering electrons forming Cooper pairs and enhance T_c, which can be proved by the peaks of $\alpha^2F(\omega)$, and integral $\lambda(\omega)$ and projection linewidth $\gamma_{\boldsymbol{q}v}$. However, the contribution from the low-frequency translational vibrations constitutes 13.64% of the integral λ. The corresponding T_c of 238 K estimated with $\mu^* = 0.1$ is close to LaH_{10} of 254 K. Particularly, the average phonon frequency $\omega_{\log}$ and λ reach 1443 K and 1.86, respectively. Compared with the vibrational characteristics and EPC of LaH_{10} at 300 GPa, the $\omega_{\log}$ of NaH_{10} is close to the 1488 K obtained for LaH_{10}, and $\lambda(\omega)$ is higher than the 1.78 calculated for LaH_{10} [15], pointing out two important factors inducing the $R32$-NaH_{10} phase to possess a high T_c. The ability of $R32$-NaH_{10} to possess a high average phonon frequency is mainly attributing to the shortest H−H bond length of only 0.78–0.80 Å, severely shorter than atomic hydrogen type Fm-$3m$-LaH_{10}, where $r_{H-H} > 1.0$ Å. The relatively large EPC of NaH_{10} prompted us to investigate the reasons affecting the intensity of electrons scattered by phonons. Next, our research mainly focuses on the analysis of the electronic properties and phonon characteristics, traced back to the Hopfield expression, $\lambda = \frac{N(\varepsilon_F)\langle I^2\rangle}{M\omega^2}$, to further unveil the features of EPC interaction and superconductivity [54].

Regarding the $N(\varepsilon_F)$ term arising from the electronic properties in Fig. 2(c), significantly, we revealed a unique mechanism of background charge participating in the EPC observed in the projected DOS, that is, valence electrons being ionized and delocalized caused by high pressure, forming a distributed environmental charge density to mediate metallic interactions. This result is completely different from the formation mechanism of interstitial quasiatoms in compressed lithium and sodium, which show insulating properties [55,56]. In fact, the increased kinetic energy of the electrons induced by pressure here exceeds the limit of the Coulomb potential field, which makes the partial charges redistribute in the lattice as background charges, and this analogous scenario also occurs in the atomic metallic H-IV phase ($I4_1/amd$) with a predicted T_c of 356 K at 500 GPa [52]. The projected DOS illustrates that high pressures induce the filling of H-p orbitals and form sp-hybridized states, which cooperate with the background charges to mainly constitute the FS. The hydrogen atoms in NaH_{10} with p-electron occupied orbitals exhibit the characteristics of 2p-block elements, implying that multiple band pairings of s- and p-electronic states cross ε_F relative to s-block element H (see Fig. S6 [34]) [57]. In Fig. S7, a large EPC also benefited from the high DOS at ε_F caused by a Van Hove singularity, which is mainly constituted with H-sp hybridized states and background charges where they make the 58% and 42% contribution to the total DOS, respectively [57,58]. These sp-hybridized states are expected to have higher freedoms of orbital multiplicity and more easily form stable Cooper pairs than H-s electrons [59,60]. Figure S10 [34] further confirmed that the background charges mainly participate in EPC due to the total $N(\varepsilon_F)$ of background charges that increased with the pressurization.

Regarding the vibrational modes of phonons reflected by the $\frac{\langle I^2\rangle}{M\omega^2}$ term as exhibited in Fig. 2(a), a striking feature of the phonon band is that various optical phonon vibrational modes have differential degrees to participate in EPC corresponding to the same $\boldsymbol{q}$-vector. The underlying causations behind this physical connotation can be revealed by the linewidth $\gamma_{\boldsymbol{q}v}$ representation. The $\gamma_{\boldsymbol{q}v}$ is primarily subjected to two factors: the nesting function $\xi(\boldsymbol{q})$ and the electron-phonon matrix element $g_{mn}(\boldsymbol{k},\boldsymbol{q})$ based on the formula $\gamma_{\boldsymbol{q}v} = \pi\omega_{\boldsymbol{q}v}\sum_{mn}\sum_{\boldsymbol{k}}|g^v_{mn}(\boldsymbol{k},\boldsymbol{q})|^2\delta(\varepsilon_{m,\boldsymbol{k}+\boldsymbol{q}} - \varepsilon_f) \times \delta(\varepsilon_{n,\boldsymbol{k}} - \varepsilon_f)$ [61]. Along the Γ to Z $\boldsymbol{q}$-route above 100 THz and at the F point of the phonon band above 80 THz (see Fig. S2 [34]), we can evidently find the softening dips. The corresponding phonon dips are attributed to the main causation induced by FS nesting, which can be verified by the nesting function $\xi(\boldsymbol{q}) = \frac{1}{N}\sum_{\boldsymbol{k},i,j}\delta(\varepsilon_{\boldsymbol{k},i} - \varepsilon_F)\delta(\varepsilon_{\boldsymbol{k}+\boldsymbol{Q},j} - \varepsilon_F)$ in Fig. 2(b). Two relatively high peaks correspond to a strong nesting strength along the Γ to Z $\boldsymbol{q}$-route and at the F point. Next, we calculate the FS to check for nesting behavior. Of particular note is that two tripodlike FSs are buckled upside down to form nesting, evidenced in Fig. 2(d). This result explains the softening dips on phonon modes caused by FS nesting. Moreover, the nature of the FS with differential Fermi velocity also affects the superconductivity. According to the relationship $\xi(\boldsymbol{q}) \propto \oint \frac{dl_{\boldsymbol{k}}}{|V_{\boldsymbol{k}} \times V_{\boldsymbol{k}+\boldsymbol{q}}|}$, the Fermi velocities of $V_{\boldsymbol{k}}$ and $V_{\boldsymbol{k}+\boldsymbol{q}}$ at ε_F are almost reverse collinear, indicating the $\xi(\boldsymbol{q})$ is stronger at the nesting points [46]. Nesting at the mentioned points certainly affects the phonon frequencies, while the nonsoftening phonon frequencies corresponding to the same $\boldsymbol{q}$-point contributing to EPC are interrelated with the $g_{mn}(\boldsymbol{k},\boldsymbol{q})$, as reflected by the thickness of the linewidth in the phonon band [62]. Thus, the phonon softening caused by FS nesting and $g_{mn}(\boldsymbol{k},\boldsymbol{q})$ are crucial factors causing a large T_c.

The properties of phonon band structures and energy band structures are closely related to the interactions between atoms, which, in turn, can be revealed by analyzing chemical bonds. We thus investigated the bonding characteristics of NaH_{10} in comparison with clathratelike hydrides LaH_{10} and YH_{10}, and insulating molecular phases of solid hydrogen at 300 GPa [63]. The bonding strengths were examined in depth through calculating the integral crystal orbital Hamilton population (iCOHP) and crystal orbital Hamilton population (COHP) of H−H pairs [64]. As Fig. 3(a) illustrates, the bonding strengths between H_2 units of NaH_{10} in the solid red line region are less than the weak covalent bond strengths in extended clathrate hydrides LaH_{10} and YH_{10}, and intramolecular bonding strengths in the solid light-blue line region are approximate or slightly less than that in pure H-III phases. These results reconfirm that the hydrogen framework is almost composed of molecular H_2 units. To explain the above-mentioned results, the COHP calculation in Fig. 3(b) indicates that the bonding molecular orbital (BMO, σ) of the H_2 molecule (0.80 Å) is completely occupied, and the antibonding molecular orbital (AMO, σ^*) is partially occupied due to the transferred electrons from sodium. Correspondingly, a small amount of electrons are distributed in the BMOs between H_2 units, which ensures the charge connectivity between them resulting in metallicity.

To further understand the superconducting behavior of the H_2 molecular type NaH_{10} with pressure, we calculated the T_c's, $\omega_{\log}$, λ, and $N\varepsilon_F$ at different pressures in Fig. 4(a). The T_c's increase as pressure increases from 168 K at

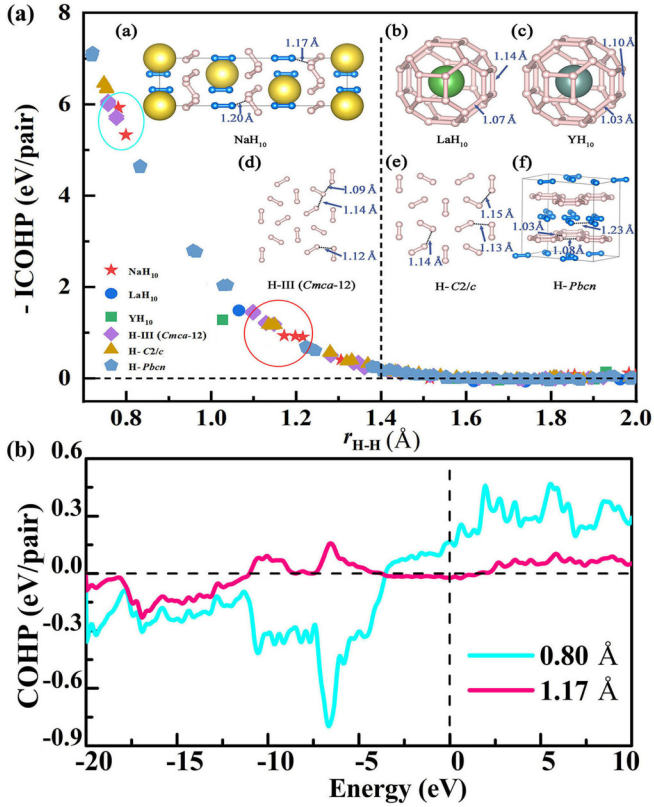

FIG. 3. (a) Calculated bond length $r_{H\text{-}H}$ and the corresponding –iCOHP values between the nearest-neighbor H atoms in different systems at 300 GPa. (b) Plot of COHP for H-H pairs separated by 0.80 Å (intramolecular distance) and 1.17 Å (intermolecular distance).

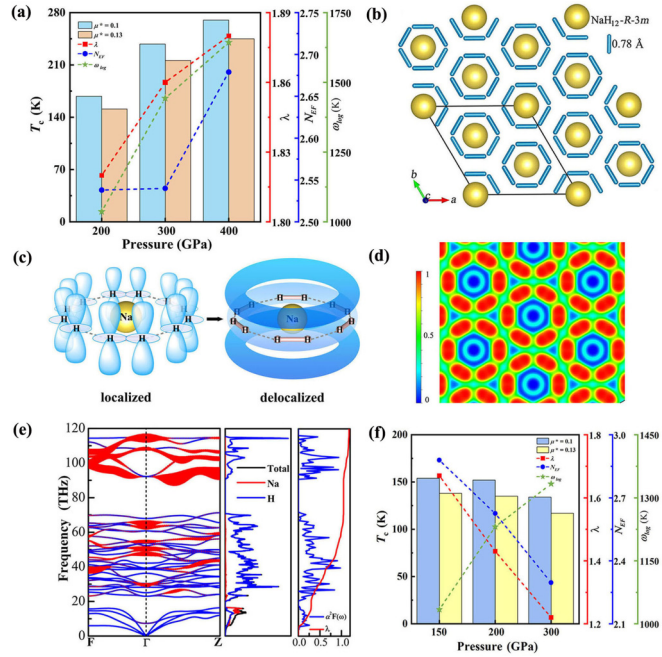

FIG. 4. (a) Calculated superconductivities for $R32$-NaH_{10} as a function of pressures. (b) R-$3m$-NaH_{12} phase at 300 GPa, (c) Energy distribution spectra of localized and delocalized sp-hybridized electrons in the Lewis structure for planar benzenelike H_{12} sublattice. (d) ELF of R-$3m$-NaH_{12}. (e) Phonon dispersion curves, $\alpha^2F(\omega)$ and integral $\lambda(\omega)$, and (f) superconductivities for R-$3m$-NaH_{12} as a function of pressures.

200 GPa to 270 K at 400 GPa. As the $R32$ phase is compressed to 400 GPa, the moderate increase of T_c is mainly brought about by the enhanced EPC, ω_{log}, and $N\varepsilon_F$. Especially in medium-frequency vibration modes (25–80 THz), the peaks of the $\alpha^2F(\omega)$ have increased (see Fig. S2 [34]). Note that the influence of medium-frequency vibrational modes on the integrated EPC has further expanded by nearly 8%, reflecting the electron-phonon matrix element driven by interatomic interactions contributing to λ continuously in a crucial manner. At 400 GPa, the abnormal performance of the optical phonon softening induced by FS nesting is increased at the F point corresponding to >80 THz, further enhancing EPC (see Fig. 2(b) and Fig. S2 [34]). Besides, $N\varepsilon_F$ increased with pressure enhancing the possibility of electrons being scattered by phonons, which increases the strength of EPC thus improving T_c. However, the effect of low-frequency modes on EPC become less significant with pressure, which suggests that T_c is very sensitive to the medium-frequency vibrational motions in this H_2 molecular type structure.

To propose more H_2 molecule type hydrides and investigate the correlation between molecular H_2 unit and high T_c, we further doped sodium into the H-III phase for computational simulation at 300 GPa. Subsequently, we obtained a dynamically stable R-$3m$-NaH_{12} structure in Fig. 4(b), which was in agreement with the previously predicted result in NaH_{12} stoichiometry [30]. The molecular H_2 units with equal bond lengths of 0.78 Å are shaped into a planar benzenelike structure composed of 12 hydrogen atoms, but intermolecular interactions are also connected by noncovalent bonds and stacked along the c axis [see Fig. 4(d)]. In sharp contrast to the insulating molecular phase H-III of solid hydrogen, R-$3m$-NaH_{12} is metallic as determined by the background charges and electrons occupying the sp-hybridized antibonding bands, which form delocalized characteristics in a planar benzenelike H_{12} sublattice. This result is supported by comparing the kinetic energy relationship in the cases of "localized or delocalized electronic states" as discussed in Fig. 4(c) and Scheme S1 [34]. Next, we conducted superconductivity and illustrated the T_c of this phase with the evolution of high pressure. The molecular-type hydride NaH_{12} also has a notable T_c of 154 K at a relatively low pressure of 150 GPa. Instructively, our observation of the emergence of H_2 molecular type hydrides with notable T_c highlights the correlation between H_2 units and novel superconductors.

In summary, we propose a high-throughput structural search approach to screen H_2 molecular type hydrides to quickly identify potential high T_c. We confirm a unique type of pressure-induced near room-temperature superconductors in solely H_2 molecule constituted NaH_{10} with T_c of 270 K at 400 GPa and NaH_{12} with high T_c of 154 K at 150 GPa, which is a prototype in the family of H_2 molecular type hydrides. Being subjected to extensive first-principles calculations, the electronic structures, bonding properties, and superconductivities of NaH_{10} and NaH_{12} are revealed. The potential near room-

temperature superconductivity originates from strong EPC to scatter itinerant electrons. The unique delocalized background charges and electrons occupying the pressure-induced *sp*-hybridized antibonding bands of molecular H_2 units act as itinerant electrons to participate in EPC. Our work reshapes the cognition of hydrogen molecular dominated superconductivity and will stimulate future high-pressure experimental work on synthesis of these H_2 molecular type structures to obtain room-temperature superconductors.

Acknowledgments. This work was supported by the National Key R&D Program of China (Grants No. 2023YFA1406200 and No. 2022YFA1405500), National Natural Science Foundation of China (Grants No. 12304021 and No. 52072188). Zhejiang Provincial Natural Science Foundation of China (Grant No. LQ23A040004), Program for Science and Technology Innovation Team in Zhejiang (Grant No. 2021R01004), Natural Science Foundation of Ningbo (Grant No. 2022J091), Program for Changjiang Scholars and Innovative Research Team in University (No. IRT_15R23), the calculations were performed in Supercomputer Center of NBU. E.Z. acknowledges the National Science Foundation (DMR-2136038) for financial support.

Z.L. and J.L. contributed equally to this work. T.C. led the project. T.C., Y.L., and Z.L. conceived the project. Z.L, J.L., J.Y., S.G., A.Z., and Q.Z. performed the calculations. Z.L., T.C., and E.Z. analyzed the data and wrote the Letter. All authors discussed the results and commented on the Letter.

The authors declare no conflict of interest.

[1] A. R. Oganov, C. J. Pickard, Q. Zhu, and R. J. Needs, Structure prediction drives materials discovery, Nat. Rev. Mater. **4**, 331 (2019).

[2] L. Zhang, Y. Wang, J. Lv, and Y. Ma, Materials discovery at high pressures, Nat. Rev. Mater. **2**, 329 (2017).

[3] N. W. Ashcroft, Metallic hydrogen: A high-temperature superconductor? Phys. Rev. Lett. **21**, 1748 (1968).

[4] R. P. Dias and I. F. Silvera, Observation of the Wigner-Huntington transition to metallic hydrogen, Science **355**, 715 (2017).

[5] C. Narayana, H. Luo, J. Orloff, and A. L. Ruoff, Solid hydrogen at 342 GPa: no evidence for an alkali metal, Nature (London) **393**, 46 (1998).

[6] E. Zurek and T. Bi, High-temperature superconductivity in alkaline and rare earth polyhydrides at high pressure: A theoretical perspective, J. Chem. Phys. **150**, 050901 (2019).

[7] D. Duan, Y. Liu, F. Tian, D. Li, X. Huang, Z. Zhao, H. Yu, B. Liu, W. Tian, and T. Cui, Pressure-induced metallization of dense $(H_2S)_2H_2$ with high-T_c superconductivity, Sci. Rep. **4**, 6968 (2014).

[8] M. Du, W. Zhao, T. Cui, and D. Duan, Compressed superhydrides: The road to room temperature superconductivity, J. Phys.: Condens. Matter **34**, 173001 (2022).

[9] D. Duan, Y. Liu, Y. Ma, Z. Shao, B. Liu, and T. Cui, Structure and superconductivity of hydrides at high pressures, Nat. Sci. Rev. **4**, 121 (2017).

[10] H. Wang, X. Li, G. Gao, Y. Li, and Y. Ma, Hydrogen-rich superconductors at high pressures, WIREs Comput. Mol. Sci. **8**, e1330 (2017).

[11] B. Lili, R. Hennig, P. Hirschfeld, G. Profet, A. Sanna, E. Zurek, W. E. Pickett, M. Amsler, R. Dias, M. I. Eremets, and C. Heil, The 2021 room-temperature superconductivity roadmap, J. Phys.: Condens. Matter **34**, 183002 (2022).

[12] K. P. Hilleke and E. Zurek, Rational design of superconducting metal hydrides via chemical pressure tuning, Angew. Chem., Int. Ed. **61**, e202207589 (2022).

[13] A. P. Drozdov, M. I. Eremets, I. A. Troyan, V. Ksenofontov, and S. I. Shylin, Conventional superconductivity at 203 kelvin at high pressures in the sulfur hydride system, Nature (London) **525**, 73 (2015).

[14] F. Peng, Y. Sun, C. J. Pickard, R. J. Needs, Q. Wu, and Y. Ma, Hydrogen clathrate structures in rare earth hydrides at high pressures: Possible route to room-temperature superconductivity, Phys. Rev. Lett. **119**, 107001 (2017).

[15] H. Liu, I. I. Naumov, R. Hoffmann, N. W. Ashcroft, and R. J. Hemley, Potential high-T_c superconducting lanthanum and yttrium hydrides at high pressure, Proc. Natl. Acad. Sci. USA **114**, 6990 (2017).

[16] M. Somayazulu, M. Ahart, A. K. Mishra, Z. M. Geballe, M. Baldini, Y. Meng, V. V. Struzhkin, and R. J. Hemley, Evidence for superconductivity above 260 K in lanthanum superhydride at megabar pressures, Phys. Rev. Lett. **122**, 027001 (2019).

[17] A. P. Drozdov, P. P. Kong, V. S. Minkov, S. P. Besedin, M. A. Kuzovnikov, S. Mozaffari, L. Balicas, F. F. Balakirev, D. E. Graf, V. B. Prakapenka, E. Greenberg, D. A. Knyazev, M. Tkacz, and M. I. Eremets, Superconductivity at 250 K in lanthanum hydride under high pressures, Nature (London) **569**, 528 (2019).

[18] P. Kong, V. S. Minkov, M. A. Kuzovnikov, A. P. Drozdov, S. P. Besedin, S. Mozaffari, L. Balicas, F. F. Balakirev, V. B. Prakapenka, S. Chariton, D. A. Knyazev, E. Greenberg, and M. I. Eremets, Superconductivity up to 243 K in the yttrium-hydrogen system under high pressure, Nat. Commun. **12**, 5075 (2021).

[19] E. Snider, N. Dasenbrock-Gammon, R. McBride, X. Wang, N. Meyers, K. V. Lawler, E. Zurek, A. Salamat, and R. P. Dias, Synthesis of yttrium superhydride superconductor with a transition temperature up to 262 K by catalytic hydrogenation at high pressures, Phys. Rev. Lett. **126**, 117003 (2021).

[20] Z. Li, Xin He, C. Zhang, X. Wang, S. Zhang, Y. Jia, S. Feng, K. Lu, J. Zhao, J. Zhang, B. Min, Y. Long, R. Yu, L. Wang, M. Ye, Z. Zhang, V. Prakapenka, S. Chariton, P. A. Ginsberg, J. Bass *et al.*, Superconductivity above 200 K discovered in superhydrides of calcium, Nat. Commun. **13**, 2863 (2022).

[21] L. Ma, K. Wang, Y. Xie, X. Yang, Y. Wang, M. Zhou, H. Liu, X. Yu, Y. Zhao, H. Wang, G. Liu, and Y. Ma, High-temperature superconducting phase in clathrate calcium hydride up to 215 K at a pressure of 172 GPa, Phys. Rev. Lett. **128**, 167001 (2022).

[22] P. Cudazzo, G. Profeta, A. Sanna, A. Floris, A. Continenza, S. Massidda, and E. K. Gross, *Ab initio* description of high-temperature superconductivity in dense molecular hydrogen, Phys. Rev. Lett. **100**, 257001 (2008).

[23] G. Ga, A. R. Ogano, P. Li, Z. Li, H. Wang, T. Cui, Y. Ma, A. Bergarad, A. O. Lyakhovb, T. Iitakag, and G. Zou, High-

pressure crystal structures and superconductivity of stannane (SnH_4), Proc. Natl. Acad. Sci. USA **107**, 1317 (2010).

[24] G. Gao, A. R. Oganov, A. Bergara, M. Martinez-Canales, T. Cui, T. Iitaka, Y. Ma, and G. Zou, Superconducting high pressure phase of germane, Phys. Rev. Lett. **101**, 107002 (2008).

[25] T. A. Strobel, M. Somayazulu, and R. J. Hemley, Novel pressure-induced interactions in silane-hydrogen, Phys. Rev. Lett. **103**, 065701 (2009).

[26] T. A. Strobel, X. J. Chen, M. Somayazulu, and R. J. Hemley, Vibrational dynamics, intermolecular interactions, and compound formation in GeH_4-H_2 under pressure, J. Chem. Phys. **133**, 164512 (2010).

[27] H. Xie, Y. Yao, X. Feng, D. Duan, H. Song, Z. Zhang, S. Jiang, S. Redfern, V. Z. Kresin, C. J. Pickard, and T. Cui, Hydrogen pentagraphenelike structure stabilized by hafnium: A high-temperature conventional superconductor, Phys. Rev. Lett. **125**, 217001 (2020).

[28] A. Shamp and E. Zurek, Superconductivity in hydrides doped with main group elements under pressure, Nov. Supercond. Mater. **3**, 14 (2017).

[29] V. V. Struzhkin, D. Y. Kim, E. Stavrou, T. Muramatsu, H. K. Mao, C. J. Pickard, R. J. Needs, V. B. Prakapenka, and A. F. Goncharov, Synthesis of sodium polyhydrides at high pressures, Nat. Commun. **7**, 12267 (2016).

[30] P. Baettig and E. Zurek, Pressure-stabilized sodium polyhydrides: $NaH_n (n > 1)$, Phys. Rev. Lett. **106**, 237002 (2011).

[31] J. Hooper and E. Zurek, High pressure potassium polyhydrides: A chemical perspective, J. Phys. Chem. C **116**, 13322 (2012).

[32] J. Hooper and E. Zurek, Rubidium polyhydrides under pressure: Emergence of the linear H_3^- species, Chem. **18**, 5013 (2012).

[33] Y. Fu, X. Du, L. Zhang, F. Peng, M. Zhang, C. J. Pickard, R. J. Needs, D. J. Singh, W. Zheng, and Y. Ma, High-pressure phase stability and superconductivity of pnictogen hydrides and chemical trends for compressed hydrides, Chem. Mater. **28**, 1746 (2016).

[34] See Supplemental Material at http://link.aps.org/supplemental/10.1103/PhysRevB.109.L180501 for detailed descriptions of the calculation methods, superconducting calculations, localized and delocalized energy characteristics in a planar benzenelike H12 sublattice, thermodynamic stability of the $R32$-NaH_{10} phase under pressure, phonon dispersion curves, selected highest-lying phonon mode displacements, and electronic band structure, which includes Refs. [35–45].

[35] G. Kresse and J. Furthmuller, Efficient iterative schemes for *ab initio* total-energy calculations using a plane-wave basis set, Phys. Rev. B **54**, 11169 (1996).

[36] P. E. Blöchl, Projector augmented-wave method, Phys. Rev. B **50**, 17953 (1994).

[37] T. Thonhauser, S. Zuluaga, C. A. Arter, K. Berland, E. Schroder, and P. Hyldgaard, Spin signature of nonlocal correlation binding in metal-organic frameworks, Phys. Rev. Lett. **115**, 136402 (2015).

[38] T. Lu and F. Chen, MULTIWFN: A multifunctional wavefunction analyzer, J. Comput. Chem. **33**, 580 (2012).

[39] P. Giannozzi, P. Giannozzi, S. Baroni, N. Bonini, M. Calandra, R. Car, C. Cavazzoni, D. Ceresoli, G. L. Chiarotti, M. Cococcioni *et al.*, QUANTUM ESPRESSO: A modular and open-source software project for quantum simulations of materials, J. Phys.: Condens. Matter **21**, 395502 (2009).

[40] G. S. Priyanga, A. T. A. Meenaatci, R. R. Palanichamy, and K. Iyakutti, Structural, electronic and elastic properties of alkali hydrides (MH: M = Li, Na, K, Rb, Cs): *Ab initio* study, Comput. Mater. Sci. **84**, 206 (2014).

[41] M. Hanfland, I. Loa, and K. Syassen, Sodium under pressure: bcc to fcc structural transition and pressure-volume relation to 100 GPa, Phys. Rev. B **65**, 184109 (2002).

[42] E. Gregoryanz, L. F. Lundegaard, M. I. McMahon, C. Guillaume, R. J. Nelmes, and M. Mezouar, Structural diversity of sodium, Science **320**, 1054 (2008).

[43] M. I. McMahon, E. Gregoryanz, L. F. Lundegaard, I. Loa, C. Guillaume, R. J. Nelmes, A. K. Kleppe, M. Amboage, H. Wilhelm, and A. P. Jephcoat, Structure of sodium above 100 GPa by single-crystal x-ray diffraction, Proc. Natl. Acad. Sci. USA **104**, 17297 (2007).

[44] Y. Li, Y. Wang, C. J. Pickard, R. J. Needs, Y. Wang, and Y. Ma, Metallic icosahedron phase of sodium at terapascal pressures, Phys. Rev. Lett. **114**, 125501 (2015).

[45] J. Klimeš, D. R. Bowler, and A. Michaelides, Chemical accuracy for the van der Waals density functional, J. Phys.: Condens. Matter **22**, 022201 (2010).

[46] J. S. Tse, Y. Yao, and K. Tanaka, Novel superconductivity in metallic SnH_4 under high pressure, Phys. Rev. Lett. **98**, 117004 (2007).

[47] E. R. Johnson, S. Keinan, P. Mori-Sanchez, J. Contreras-Garcia, A. J. Cohen, and W. T. Yang, Revealing noncovalent interactions, J. Am. Chem. Soc. **132**, 6498 (2010).

[48] X. Zhong, H. Wang, J. Zhang, H. Liu, S. Zhang, H. F. Song, G. Yang, L. Zhang, and Y. Ma, Tellurium hydrides at high pressures: High-temperature superconductors, Phys. Rev. Lett. **116**, 057002 (2016).

[49] W. H. Sun, S. T. Dacek, S. P. Ong, G. Hautier, A. Jain, W. D. Richards, A. C. Gamst, K. A. Persson, and G. Ceder, The thermodynamic scale of inorganic crystalline metastability, Sci. Adv. **2**, e1600225 (2016).

[50] C. Liu, H. Gao, A. Hermann, Y. Wang, M. Miao, C. J. Pickard, R. J. Needs, H. Wang, D. Xing, and J. Sun, Plastic and superionic helium ammonia compounds under high pressure and high temperature, Phys. Rev. X **10**, 021007 (2020).

[51] P. B. Allen and R. C. Dynes, Transition temperature of strong-coupled superconductors reanalyzed, Phys. Rev. B **12**, 905 (1975).

[52] J. M. McMahon and D. M. Ceperley, Ground-state structures of atomic metallic hydrogen, Phys. Rev. Lett. **106**, 165302 (2011).

[53] Y. Sun, Y. Tian, B. Jiang, X. Li, H. Li, T. Iitaka, X. Zhong, and Y. Xie, Computational discovery of a dynamically stable cubic SH_3-like high-temperature superconductor at 100 GPa via CH_4 intercalation, Phys. Rev. B **101**, 174102 (2020).

[54] N. I. Kulikov, McMillan-Hopfield factor and ideal resistivity of transition metals, J. Phys. F: Met. Phys. **8**, L137 (1978).

[55] Y. Ma, M. Eremets, A. R. Oganov, Y. Xie, I. Trojan, S. Medvedev, A. O. Lyakhov, M. Valle, and V. Prakapenka, Transparent dense sodium, Nature (London) **458**, 182 (2009).

[56] J. Lv, Y. Wang, L. Zhu, and Y. Ma, Predicted novel high-pressure phases of lithium, Phys. Rev. Lett. **106**, 015503 (2011).

[57] C. Wang, S. Yi, and J.-H. Cho, Multiband nature of room-temperature superconductivity in LaH_{10} at high pressure, Phys. Rev. B **101**, 104506 (2020).

[58] H. Wang, J. S. Tse, K. Tanaka, T. Iitaka, and Y. Ma, Superconductive sodalite-like clathrate calcium hydride at high pressures, Proc. Natl. Acad. Sci. USA **109**, 6463 (2012).

[59] Y. Kohama, S. W. Kim, T. Tojo, H. Kawaji, T. Atake, S. Matsuishi, and H. Hosono, Evidence for Bardeen-Cooper-Schrieffer-type superconducting behavior in the electride $(CaO)_{12}(Al_2O_3)_7$: e^- from heat capacity measurements, Phys. Rev. B **77**, 092505 (2008).

[60] N. E. Christensen and D. L. Novikov, Predicted superconductive properties of lithium under pressure, Phys. Rev. Lett. **86**, 1861 (2001).

[61] Y. Ma, D. Duan, Z. Shao, H. Yu, H. Liu, F. Tian, X. Huang, D. Li, B. Liu, and T. Cui, Divergent synthesis routes and superconductivity of ternary hydride $MgSiH_6$ at high pressure, Phys. Rev. B **96**, 144518 (2017).

[62] Y. Ma, J. S. Tse, D. D. Klug, and R. Ahuja, Electron-phonon coupling of α-Ga boron, Phys. Rev. B **70**, 214107 (2004).

[63] C. J. Pickard and R. J. Needs, Structure of phase III of solid hydrogen, Nature (London) **3**, 473 (2007).

[64] R. Dronskowski and P. Blöchl, Crystal orbital Hamilton populations (COHP): Energy-resolved visualization of chemical bonding in solids based on density-functional calculations, J. Phys. Chem. A **97**, 8617 (1993).